Microwave Combustion Synthesis of Silver Doped Lanthanum Ferrite Magnetic Nanoparticles

P.A. Desai and Anjali A. Athawale[*]

University of Pune, Pune–411 007, India
[*]*Centre for Nanoscience and Quantum Systems, Pune–411 007, India*
[*]*E-mail: agbed@chem.unipune.ac.in*

ABSTRACT

Lanthanum ferrite ($LaFeO_3$) and silver doped $LaFeO_3$ powders were synthesized by a single step microwave combustion route using nitrates as precursors and glycine as a fuel. XRD analysis indicated the formation of cubic phase with the dopant peaks at 2θ values of 38.3°, 44.1°, and 64.4° apart from the peaks corresponding to $LaFeO_3$. As observed from the transmission electron micrographs, $LaFeO_3$ exhibits particles with a larger size (mean size ~57 nm), significant decrease in particle size is observed for silver doped samples. The magnetic measurements reveal weak ferromagnetic nature of $LaFeO_3$, while silver doped samples are ferromagnetic in nature. Lanthanum silver ferrite (x = 0.25, A site) shows maximum coercivity (Hci = 480.96 G) with hysteresis loop at room temperature which is a clear sign of ferromagnetic ordering. The S shape of the curve implies the presence of domain wall movements in nanoparticles. Thermogravimetric analysis of the samples show stable behavior of the products.

Keywords: Microwave processing, electron microscopy, magnetic properties, perovskites

1. INTRODUCTION

Lanthanum ferrite ($LaFeO_3$) is a functional ceramic with 12:6 co-ordinate perovskite structure, which was first synthesized by Koehler and Wollan[1] in 1957. It is extensively used as an interconnect for SOFC's, catalytic converter and more recently as a sputtering target[2]. Doping this, further enhances its technological applicability. Alkali and alkaline earth metals are the commonly used dopants[3]. However, doping with noble metals improves its catalytic activity due to increase in oxygen ion vacancies. Few reports are available on silver doping with sub micron particles/flakes[4-6] with orthorhombic crystal structure. The ionic and electronic defects are seen to govern the properties of functional ceramics[7-8]. Several chemical methods have been used to synthesize lanthanum orthoferrite such as polymerizable complex route[9,10], electro spinning technique[11,12], sol-gel[13], auto combustion route[14], sonochemical synthesis[15,16], solid state reaction[17], combustion[18] etc. However, these methods of synthesis require heat treatment with chelating agent and complex solutions to yield pure products. Additionally, some exhibit slow reaction rate, prolonged reaction time, heating inhomogeneity, and excessive energy consumption.

The present work, reports for the first time the microwave combustion route to synthesize nanoparticles of silver doped lanthanum ferrite with cubic crystal geometry. The tolerance factor of 0.95 for lanthanum ferrite (Goldschmidt tolerance factor) confirms the cubic geometry as well as stability of the phase. The decrease in the tolerance factor in doped samples indicates distortion in FeO_6 octahedra due to silver ions. Phase pure products with high degree of crystallinity are obtained within a short reaction time of few minutes. Metallic nitrates were used as oxidizer with glycine as a fuel. The nanolanthanum silver ferrite particles are spherical in shape with a narrow size distribution.

2. EXPERIMENTAL DETAILS

All the chemicals used were of A.R. grade. The salt precursors i.e. lanthanum nitrate ($La(NO_3)_3.6H_2O$) and ferric nitrate ($Fe(NO_3)_3.9H_2O$) and glycine (NH_2CH_2COOH) as a fuel were from Loba Chemie, India, while silver nitrate ($AgNO_3$) was from Qualigens, India. Lanthanum ferrite ($LaFeO_3$) was synthesized by initially mixing the precursor salts together in stoichiometric amounts i.e. 1:1 equimolar ratio (0.08 M each) followed by addition of glycine as fuel (0.26 M). To this, were added ~50 ml of double distilled water. The stoichiometric composition of the mixture was calculated based on oxidizing valency of metal nitrates and reducing valency of glycine[19]. Silver doped samples both at A (*La*) site and B (*Fe*) site i.e. $La_{(1-x)}Ag_xFeO_3$ and $LaFe_{(1-x)}Ag_xO_3$ were prepared by partial substitution of host atoms (La and Fe) by varying the concentration of added silver (x = 0.25, 0.50, and 0.75). The resulting mixtures (for undoped and doped perovskites) were stirred for few minutes at room temperature and subjected to evaporation on a hot plate so as to obtain a gel. The gels were subjected to microwave power (0.1– 0.9 kW) using a domestic microwave oven (MG-555F Model) for auto combustion and the resulting products were cooled to room temperature. Pure phase products both, for pure and silver doped samples were obtained at 0.42 kW microwave power. During synthesis, the

fuel to oxidizer ratio was maintained as 1 while, the irradiation time was varied from 5-10 min so as to obtain pure phase products. Irradiation time of 10 min was found to be optimum yielding pure phase products. The powders were characterized using various analytical techniques.

3. CHARACTERIZATION

Fourier Transform Infrared Spectra (FTIR) of all the samples were recorded on a Shimadzu 8400 spectrophotometer over the range of 400 cm^{-1} to 4000 cm^{-1}. X-ray diffraction analysis of the powders were carried out on a PANalytical X'Pert Pro MPD X-ray Diffractometer with a monochromatic CuKα radiation (λ=1.5406Å). Silicon was used as an external standard for correction due to instrumental broadening. Diffraction data were collected from 20° to 80°. Energy Dispersive Analysis of X-rays (EDAX) were taken on an analytical instrument (JEOL JSM 6360A). The data were recorded by coating the films of the samples with *Ag-Pd* alloy using vapor deposition technique. Transmission electron micrographs (TEM's) of the samples were observed on a Philips CM-200 instrument at an accelerating voltage of 200 kV. Suspensions of the samples in isopropanol were well dispersed and loaded on carbon coated grids of 200 mesh size. The grids were then dried under IR lamp and viewed under the microscope. The Thermogravimetric and differential thermograms (TG-DTA) of the samples were recorded in inert atmosphere at a heating rate of 10 °C min^{-1} using Shimadzu instrument (Model DTG-60H). Lakeshore's Vibrating Sample Magnetometer (Model 7307) was used to perform magnetic measurements.

4. RESULTS AND DISCUSSION

The microwave combustion route involves self sustained reaction between an oxidizer, typically precursor salts of nitrates and glycine (reducing agent) as a fuel after dissolution in water. Highly exothermic reaction occurs with iron and lanthanum precursors in the viscous liquid and the complex mixture self ignites and promotes nucleation and growth of nanoparticles within short duration of time with evolution of a large amount of gas yielding fine particles of lanthanum ferrite and silver doped lanthanum ferrite.

The powder samples of $LaFeO_3$, $La_{(1-x)}Ag_xFeO_3$, $LaFe_{(1-x)}Ag_xO_3$, were characterized using various analytical techniques.

5. FTIR SPECTROSCOPY

Figure 1 (a) shows the FTIR spectrum of lanthanum ferrite. The presence of metal oxygen bonds i.e. *O-Fe-O* and *Fe-O* could be revealed from the peaks at 560 cm^{-1} and 400 cm^{-1} respectively. The band's at 3400 cm^{-1} and 3600 cm^{-1} correspond to strong vibrations of OH due to adsorbed water, while the narrow bands at 1085 cm^{-1} to 1385 cm^{-1} correspond to NO_3^- of unreacted precursor salts and N-H stretching is observed at 1485 cm^{-1}.

In Fig. 1 (b) and 1(c) are given the FTIR spectra of silver doped (both A and B site), lanthanum ferrite samples which exhibit similar nature. The *Ag* content does not result in any significant shift in peaks.
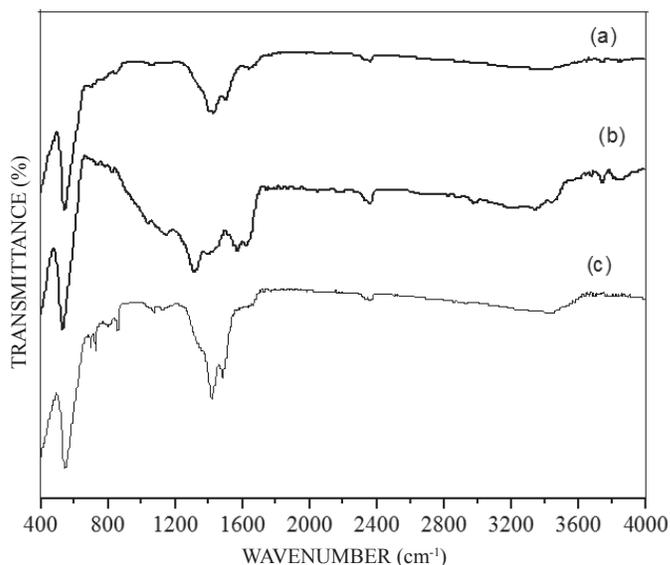

Figure 1. FT-IR spectra of samples (a) $LaFeO_3$, (b) $La_{0.75}Ag_{0.25}FeO_3$, (c) $LaFe_{0.75}Ag_{0.25}O_3$.

6. X-RAY DIFFRACTION ANALYSIS

The X-ray diffractogram of lanthanum ferrite obtained at 0.42 kW microwave power is shown in Fig. 2. The peaks at 2θ values of 22.7°, 32.2°, 39.9°, 46.2°, 67.5°, and 76.7° represent characteristic planes (100, 110, 111, 200, etc.) of Cubic (primitive) phase of $LaFeO_3$ (PDF No.75-0541). X-ray diffractograms of Ag doped (both A and B site) LaFeO$_3$ are shown in Figs. 3 and 4. The dopant concentration was varied from x = 0.25 to 0.75. Peaks corresponding to metallic silver are observed at 2θ values of 38.3°, 44.1°, and 64.4° in addition to characteristic peaks of lanthanum ferrite. The data has been correlated with JCPDS pattern (04-783). Further, increment in the intensity of the peak corresponding to silver is observed with the increase in dopant concentration.
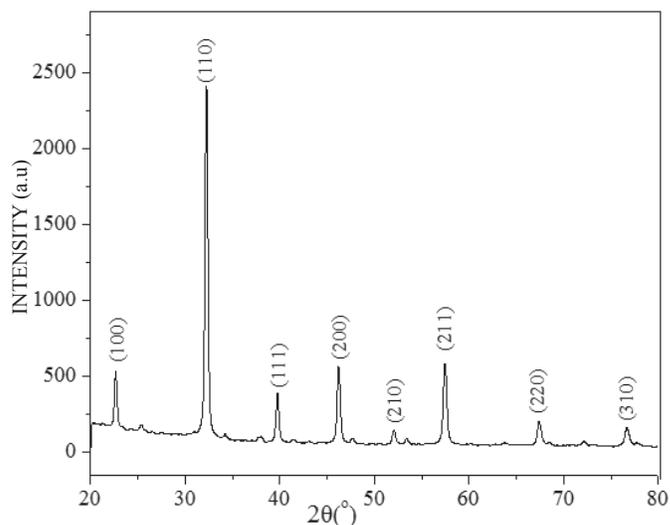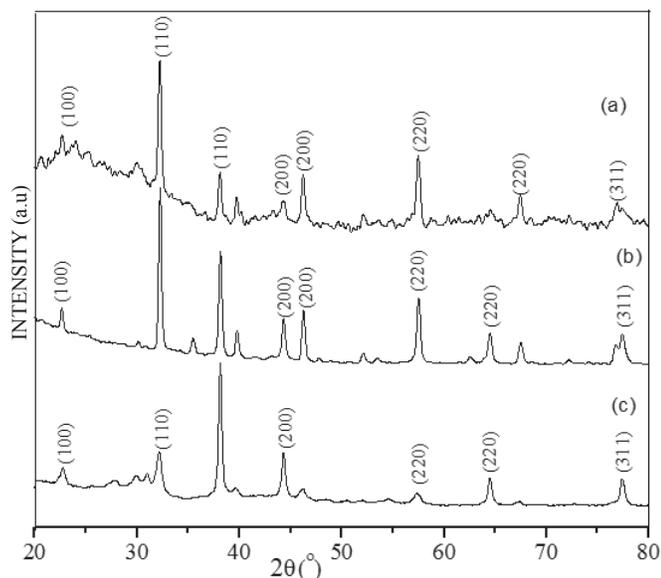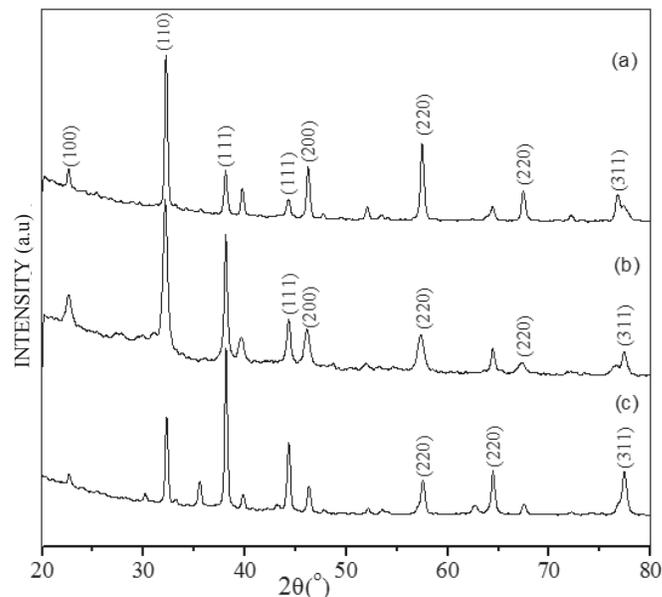

Figure 2. X-ray diffractogram of Lanthanum Ferrite sample synthesized at 0.42 kW microwave power.

Figure 3. X-ray diffractograms of Lanthanum Ferrite with silver doped at A site (a) x = 0.25, (b) x = 0.50, and (c) x = 0.75.

Figure 4. X-ray diffractograms of Lanthanum Ferrite with silver doped at B site X=0.25 (b) x=0.50 and (c) x=0.75.

The X-ray densities and crystallite size of the particles are calculated from the XRD data (Table 1), and dopant concentration expressed as a fraction with reference to host atoms. Further, the lattice parameters were evaluated which exhibit significant differences on Ag doping in comparison to $LaFeO_3$. The results indicate contraction in cell volume for A site doped (Ag, x = 0.25, 0.50 and 0.75) samples while B site dopant shows expansion in volume. This can be attributed to the mismatch of ionic radii and co-ordination number (i.e. dodecahedron and octahedra). The increment in x-ray densities results in partial site occupancy of silver as a dopant in lanthanum ferrite structure which associates with lattice contraction at A site and lattice expansion at B site. Goldschmidt tolerance factor[20] exhibits changes in geometric tolerance for lanthanum perovskites and cubic structure occurs[21,22] if 0.8 < t< 1. In accordance with this, the tolerance factor (t) for Lanthanum ferrite (undoped) is found to be ~0.958 (Table 1) while for silver doped samples (A as well as B site) lower values of t indicate distortion in crystal structure.

The results of Energy Dispersive Analysis of X-rays (EDAX) are summarized in (Table 2), the atomic ratio for La/Fe is expected to be 1, but, lanthanum ferrite shows the formation of lanthanum rich phase due to diffusion and non storage capacity of trivalent lanthanum metal in nonstoichiometric structure. Partial substitution of dopant at A site with lower fraction (x = 0.25) exhibits a hyperstoichiometry with a slight ferric ion deficiency while, at higher doping levels ferric ion enrichment is observed.

Results of the EDAX analysis of samples with B site doping (Table 2) clearly shows the formation of silver rich phase of the perovskite at lower doping level (x = 0.25 and 0.50) while at higher concentration of silver (x = 0.75) iron deficiency matches with silver concentration and oxygen abundance. Thus, this analysis determines the solid phase concentrations of elements in the sample, the discrepancy in the quantitative data is attributable to reduction ability of iron with increment in oxygen vacancies[6].

Table 1. Calculated lattice parameters of $LaFeO_3$, Lanthanum Ferrite with silver doped at A site (0.25, 0.50, and 0.75) and Lanthanum Ferrite with silver doped at B site (0.25, 0.50, and 0.75)

Perovskite	VCell a³ (m³)x 10⁻²⁹	X-ray density g/cm³	Crystallite size (nm)	Particle size (nm)	Magnetic diameter (nm)	Tolerance factor
$LaFeO_3$	5.97	6.69	~57	~57	51.2	0.958
$La_{0.75}Ag_{0.25}FeO_3$	4.62	7.75	~20	~3	~6	0.951
$La_{0.50}Ag_{0.50}FeO_3$	7.78	8.77	~15	-	-	0.615
$La_{0.25}Ag_{0.75}FeO_3$	4.62	7.60	~18	~6	~7	0.937
$LaFe_{0.75}Ag_{0.25}O_3$	7.78	7.94	~16	~5	~6	0.887
$LaFe_{0.50}Ag_{0.50}O_3$	7.78	8.07	~14	-	-	0.732
$LaFe_{0.25}Ag_{0.75}O_3$	6.4	8.20	~20	~20	~7	0.775

Table 2. EDAX data of *LaFeO₃*, Lanthanum Ferrite with silver doped at A site (x = 0.25, 0.50, and 0.75) and Lanthanum Ferrite with silver doped at B site (x = 0.25, 0.50, and 0.75).

| Perovskite	Elemental composition (atomic %)							
	Experimental				Expected			
	La	Fe	O	Ag	La	Fe	O	Ag
$LaFeO_3$	12.76	11.80	75.44	-	6.50	6.50	86.81	-
$La_{0.75}Ag_{0.25}FeO_3$	4.57	2.84	91.92	0.66	5.19	6.55	86.88	1.63
$La_{0.50}Ag_{0.50}FeO_3$	3.67	16.42	6.89	6.41	1.25	2.50	95.00	1.25
$La_{0.25}Ag_{0.75}FeO_3$	2.55	8.45	84.20	4.20	1.61	6.45	87.00	4.83
$LaFe_{0.75}Ag_{0.25}O_3$	17.61	17.73	62.28	2.37	6.74	5.05	86.51	1.68
$LaFe_{0.50}Ag_{0.50}O_3$	14.90	7.50	5.43	5.50	2.30	1.25	95.00	1.25
$LaFe_{0.25}Ag_{0.75}O_3$	5.79	1.78	89.78	2.65	6.89	2.01	86.20	5.17

7. MORPHOLOGICAL CHARACTERIZATION

Figure 5(a) shows the TEM image of *LaFeO₃*, with irregular shaped particles (mean diameter of ~ 57 nm) and clear grain boundaries are observed together with several voids (~5 nm). The size distribution appears to be broad ~ 30 to 100 nm shown in the bar diagram with majority being larger and the ring pattern exhibits polycrystalline nature of the sample Figs. 6(a) and 6(b).
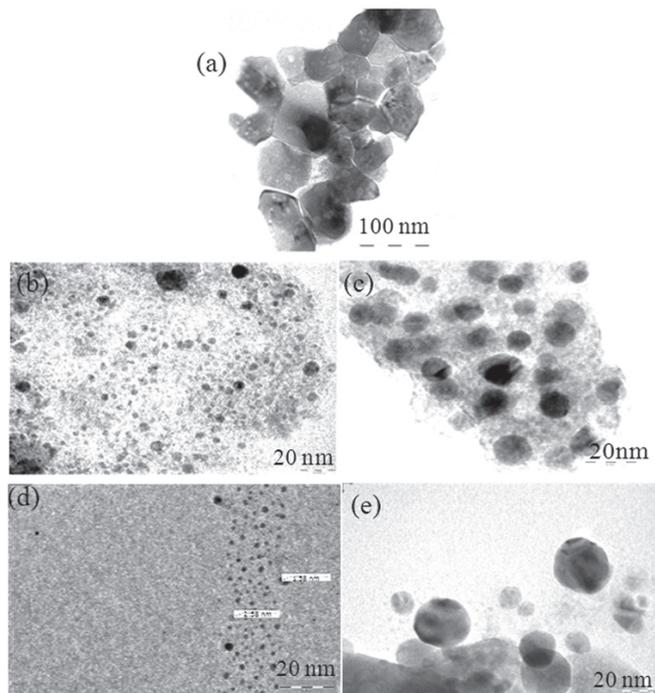
Figure 5. Transmission electron micrographs of (a) LaFeO₃, (b) and (c) A site doped $La_{(1-x)}Ag_xFeO_3$ (x = 0.25 and 0.75) and (d) and (e) B site doped $LaFe_{1x}Ag_xO_3$ (x = 0.25 and 0.75).

Micrograph of samples with silver doped at A site (x = 0.25 and 0.75) are shown in Fig. 5 (b) and 5 (c), respectively. The particles in both the samples are spherical in shape, the size being significantly smaller in comparison to pure lanthanum ferrite. The average size of particles is ~ 3 and 6
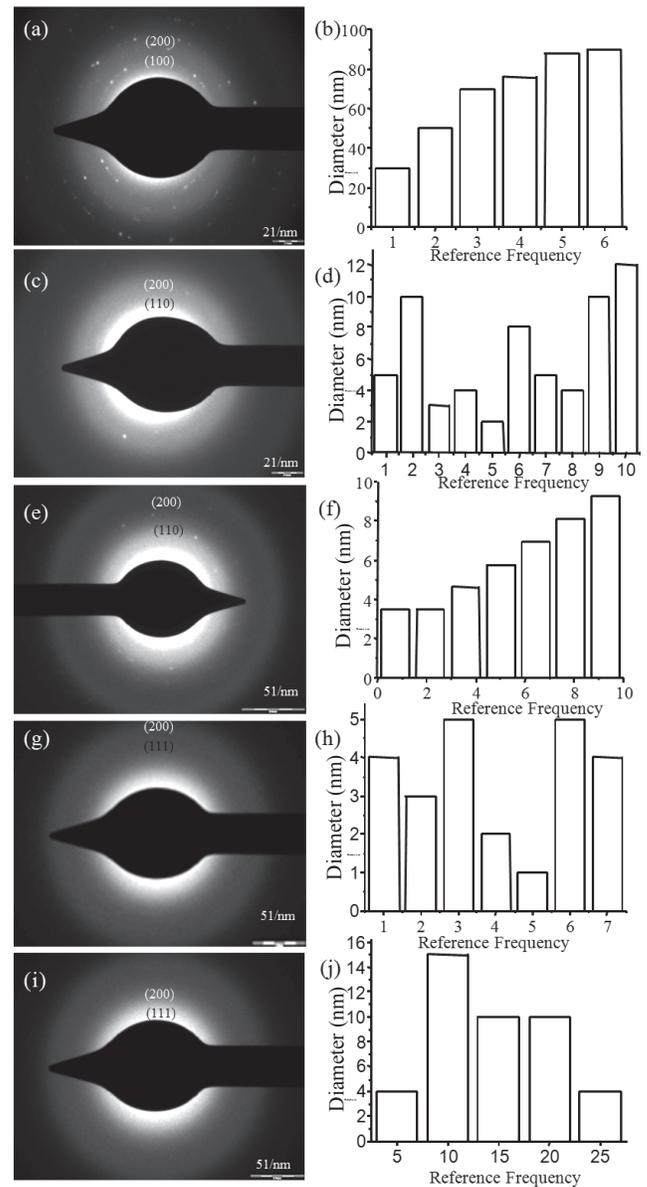
Figure 6. SAED and size distribution profiles of (a) and (b) *LaFeO₃*, A site doped $La_{1-x}Ag_xFeO_3$ (c) and (d) x = 0.25, (e) and (f) x = 0.75, and B site doped $LaFe_{(1-x)}Ag_xO_3$ (g) and (h) x = 0.25 and (i) and (j) x= 0.75.

nm respectively. The relative abundance of smaller particles being higher at x = 0.25 doping level. Particle size distribution shows slight differences and diffraction pattern exhibits array of spots related to de Broglie wavelength and polycrystallinity of the sample Figs. 6 (c) - 6 (f).

Figure 5(d) and 5(e) depicts the micrographs of lanthanum ferrite with silver doped at B site. Particles with spherical morphology can be observed from the micrographs having a size distribution of ~ 1-7 nm and ~ 5-25 nm respectively for x = 0.25 and x = 0.75 silver concentration. The diffraction patterns depict the polycrystalline nature of the samples Figs. 6(g) - 6(j).

The decrease in particle size in case of doped samples can be accounted in terms of distortion in structure brought about by the dopant ions and change in lattice dimensions.

8. THERMAL ANALYSIS

The thermograms (curves a) for $LaFeO_3$, $La_{0.75}Ag_{0.25}FeO_3$ and $LaFe_{0.75}Ag_{0.25}O_3$, are shown in Fig. 7, negligible weight loss of 1-2% is noted which can be attributed to trace levels
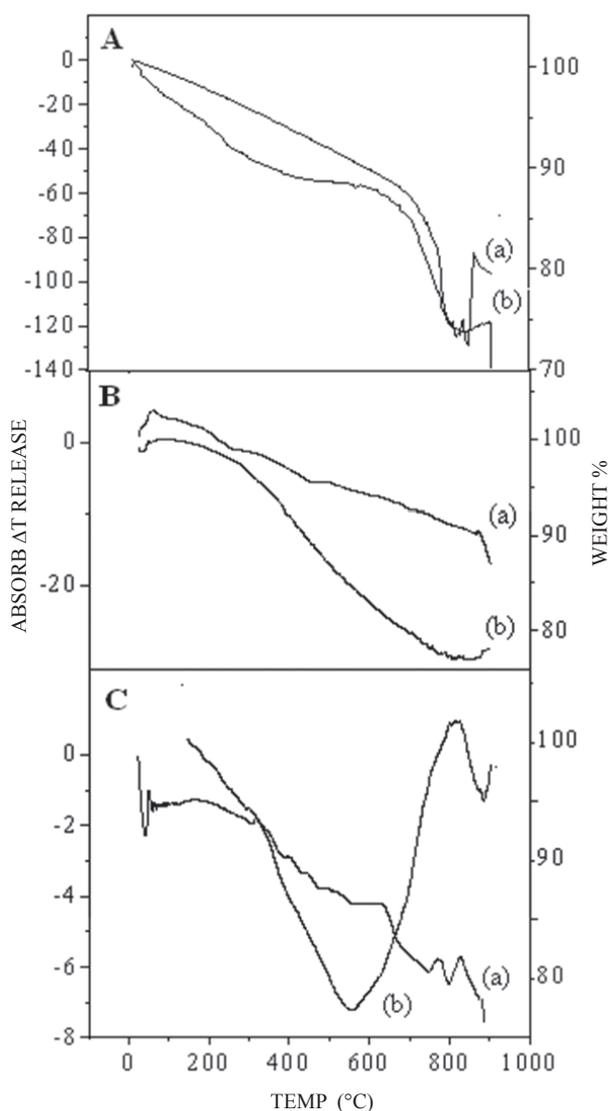
of volatiles including adsorbed water, etc. Differential thermograms (curves b) exhibit an endotherm at 90 °C corresponding to desorption of adsorbed water. The endotherm at temperature ~ 600 °C is attributable to the decomposition of traces of precursors and organic fuel (glycine) and endotherm at temperature ~ 850 °C is attributed to the gradual crystallization of oxide phase nuclei in pure as well as doped lanthanum ferrite samples.

9. MAGNETIC MEASUREMENTS

Magnetic hysteresis loops were recorded at room temperature by vibrating sample magnetometer for lanthanum ferrite and silver doped lanthanum ferrite samples as shown in Fig. 8. When an external field is applied, the domains already aligned in the direction of field grow at the expense of their neighbours. The coercivity (Hci), retentivity (Mr), and saturation magnetization (Ms) obtained for the samples are given in Table 3. The coercivity (Hci) and saturation magnetization (Ms) observed for lanthanum ferrite is 82.69 G and 4.73emug[-1] indicating weak ferromagnetic behavior that arises due to structural distortion related to tilt in FeO_6 octahedra, the results are in agreement with the reported values[23-25]. However, predominant mechanism for weak (Parasitic) ferromagnetism in the orthoferrites appears to be anisotropic super exchange (antisymmetric super exchange)[26.] The contribution of magneto crystalline anisotropy in sample with substitution of silver at A site (x = 0.25) enhances coercivity (480.96 G) due to spherical

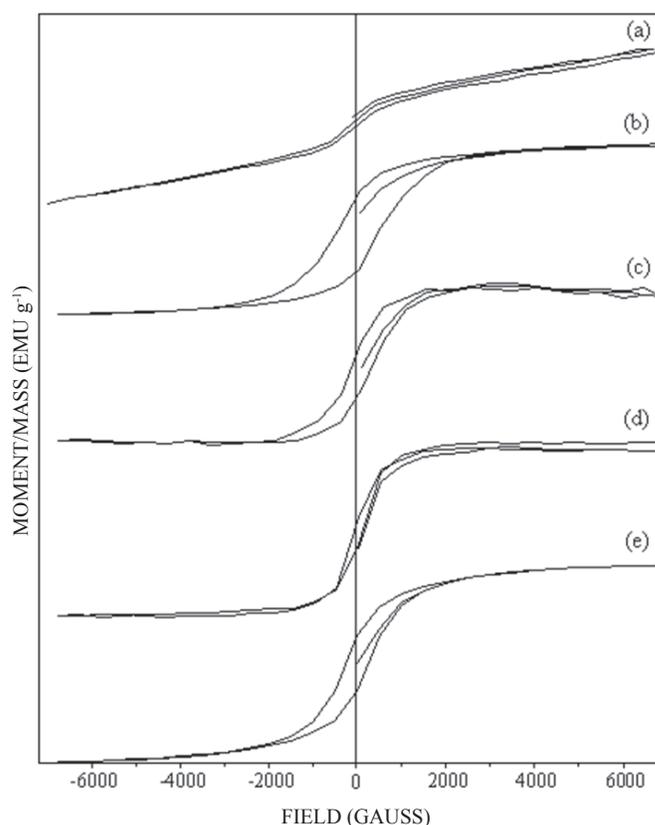Figure 7. TG (a) and DTA (b) plots of (A) $LaFeO_3$, (B) $La_{0.75}Ag_{0.25}FeO_3$, and (C) $LaFe_{0.75}Ag_{0.25}O_3$.

Figure 8. Magnetograms of (a) $LaFeO_3$, (b) $La_{0.75}Ag_{0.25}FeO_3$ (c) $La_{0.25}Ag_{0.75}FeO_3$, (d) $LaFe_{0.75}Ag_{0.25}O_3$, and (e) $LaFe_{0.25}Ag_{0.75}O_3$.

Table 3. **Magnetic data of** *LaFeO₃,* **Lanthanum ferrite with silver doped at A site (x = 0.25 and 0.75) and Lanthanum ferrite with silver doped at B site (x = 0.25 and 0.75)**

Perovskite	Saturation magnetization (Ms), E-3 emu g⁻¹	Retentivity (Mr), E-3 emu g⁻¹	Coercivity (Hci), G (Gauss)	Magnetic moment, μ_B
$LaFeO_3$	47.360	1.850	82.00	2.590
$La_{0.75}Ag_{0.25}FeO_3$	0.470	0.210	480.96	6.690
$La_{0.25}Ag_{0.75}FeO_3$	0.087	0.032	313.00	0.110
$LaFe_{0.75}Ag_{0.25}O_3$	0.110	17.780	93.00	0.580
$LaFe_{0.25}Ag_{0.75}O_3$	0.002	0.001	361.00	0.002

shape of particles with compositional homogeneity however, higher dopant concentration of silver at A site (x = 0.75) decreases coercivity due to lose magnetic neighborhood causing hysteresis loss. Further, silver substitution at B site (x = 0.25) shows a negligible change in coercive force, increase in the coercive force at higher concentration of silver at B site (0.75) can be attributed to the structural changes in the lattice arising due to different orbital configuration of Fe ions. The lower values of Ms i.e. saturation magnetization for doped samples can be accounted in terms of nonmagnetic nature of silver ions. At higher dopant concentration of silver at A as well as B site, the lattice gain their magnetic neighbourhood and hence the spin may become coupled hence, lower field is required to saturate i.e. to align the magnetic moments in the direction of applied magnetic field. The retentivity (Mr) is observed to be lower for doped samples compared to pure lanthanum ferrite except the sample doped with x = 0.25 of silver at B site. These results are consistent with the hysteresis loop arising from the demagnetization effects. However, shape anisotropy is much greater and more effective in the demagnetization together with diameter of the particles. The difference observed in retentivity for sample doped with x = 0.25 silver at B site may be due to decrease in symmetry resulting in polycrystalline nature of the sample which competes with compositional homogeneity of the sample. Further, the lower values of magnetic moments observed for doped samples with compared to pure lanthanum ferrite could be due to lower degree of magnetic interaction between the co-ordinated cations and dopant ions. The exceptional behavior of the sample doped with x = 0.75 silver at A site is probably due to site occupancy of host ions by the silver ions as a dopant. By varying the concentration of silver ions in the lanthanum ferrite system the change in the magnetic moments is a cause for changes occurring in the magnetic properties of the doped lanthanum ferrites. The magnetic moment per formula unit in Bohr magnetrons (μ_B) has been calculated by using molecular mass, saturation magnetization observed from hysteresis loops taken at room temperature and observed density of the samples[27]. Thus, hysteresis loop is characterized with Rayleigh region and microscopic rotation along with domain wall movements. Silver used as a dopant in lanthanum ferrite lattice shows that electronic distribution adopts a configuration which minimizes its interaction with crystal field and values of magnetization are strongly modified. These results indicate that the magnetic structure changes from weak ferromagnetic for pure lanthanum ferrite to ferromagnetic in case of doped samples.

The magnetic particle diameter, Dm, have been calculated using the molar magnetic susceptibility (χ_i) and saturation magnetization (Ms) values obtained from the magnetograms[28,29]. The calculated magnetic diameter is slightly smaller than that estimated from TEM for pure lanthanum ferrite as shown in Table 1. Silver doped samples reveal slightly larger magnetic diameters than that obtained from TEM. The slight difference in magnetic size can be attributed to the non-homogeneity in particle surface and crystal anisotropy[30].

10. CONCLUSION

Microwave combustion synthesis is a single step approach to synthesize magnetic nanoparticles of lanthanum ferrite and silver doped lanthanum ferrite. Structural characterization such as X-ray diffraction confirms cubic phase of the samples. Lanthanum ferrite as well as doped samples follow structural distortion and tolerance factor. Morphological evidence shows sub-micron particle size for lanthanum ferrite and silver doped samples exhibit nanospheres with compositional homogeneity. Room temperature magnetic study reveals weak ferromagnetic behavior for lanthanum ferrite sample and ferromagnetic rectangular loop formation for silver doped samples.

REFERENCES

1. Koehler, W.C. & Wollan, E.O. Neutron-diffraction study of the magnetic properties of perovskite like compounds $LaBO_3$. *J. Phys. Chem. Solids.*, 1957, **2**(2), 100-106.
2. Sun, C.; Hui, R. & Roller, J. Cathode materials for solid oxide fuel cells. *J. Solid State Electrochem.*, 2010, **14** (7)**,** 1125–1144.
3. Cheng, J. & Navrotsk, A. Thermo chemistry of $La_{1-x}Sr_xFeO_{3-\delta}$ solid solutions ($0 \le x \le 1.0, 0.0 \le \delta \le 0.5$). *Chem. Mater.*, 2005, **17** (8)**,** 2197-2207.
4. Bellakki, M.B.; Kelly, B.J. & Manivannan, V. Synthesis

characterization and property studies of *(La, Ag)FeO₃* ($0.0 \leq x \leq 0.3$) perovskites, *J. Alloys. Compd.*, 2010, **489** (1)**,** 64–71.

5. Choudhary, V.R.; Uphade, B.S. & Pataskar, S.G. Low temperature complete combustion of methane over Ag-doped *LaFeO₃* and *LaFe₀.₅Co₀.₅O₃* perovskite oxide catalysts. *Fuel*,1999, **78** (8)**,** 919–21.

6. Riosco, F.; Radov, L.; Gordon, X. Garci & Pecchi, G. Effect of Ag addition on thermal stability and catalytic properties of *LaFeO₃* perovskite, *J. Chil. Chem. Soc.*, 2010, **55** (1)**,** 44-49.

7. Kersen, Ülo. Microstructural and surface characterization of solid state sensor based on $LaFeO_{3-\delta}$ oxide for detection of NO_2. *Analyst*, 2001, **126**(8), 1377–81.

8. Jones, A. & Islam, M.S. Atomic scale insight into LaFeO₃ perovskite defect nanoclusters and ion migration. *J. Phys. Chem. C.*, 2008, **112** (12), 4455-62.

9. Popa, M.; Frantti, J. & Kakihana, M. Lanthanum ferrite $LaFeO3_{+\infty}$ nanopowders obtained by the polymerizable complex method, *Solid State Ionics.*, 2002, **154-55**, 437-45.

10. Ryu, K.H.; Im, J.E.; Wang, K.K.; Heo, E.; Lee, S.H. & Kim, Y.R. Preparation of porous LaFeO₃ nanowires using AAO template and their catalytic properties. *Bull. Korean. Chem. Soc.*, 2011, **32** (7), 1-4.

11. Dong, X.; Wang, J.; Guixia, Liu Q.C. & Yu, W. Preparation of LaFeO₃ porous hollow nanofibers by electrospinning. *Int. J. Chem.*, 2009, **1** (1), 13-17.

12. Leng, J.; Li, S.; Wang, Z.; Xue, Y. & Xu, D. Synthesis of ultrafine lanthanum ferrite (LaFeO₃ fibers via electro. spinning. *Mat. Lett.*, 2010, **64** (17)**,**1912-14.

13. Kuznetsov, M.V.; Pankhurst, Q.A.; Parkinc, I.P. & Morozova, Y.G. Self Propagating high-temperature synthesis of chromium substituted lanthanum orthoferrites $LaFe_{1-x}Cr_xO_3$ (o≤x≤1). *J. Mat. Chem.*, 2001, **11** (3), 854-858.

14. Parida, K.M.; Reddy, K.H.; Martha, S.D.; Das, P. & Biswal, N. Fabrication of nanocrystalline LaFeO₃: an efficient sol gel auto-combustion assisted visible light responsive photocatalyst for water decomposition. *Int. J. Hydration energy*, 2010, **35** (22)**,** 12161-168.

15. Wang, J.; Liu, Q. Xue, D. & Li, F. Synthesis and characterization of LaFeO₃ nano particles. *J. Mat. Sci. Lett.*, 2002, **21** (13), 1059 -1062.

16. Sivakumar, M.; Gedanken, A.; Zhong, W.; Jiang, Y.H.; Du, Y.W. Sonochemical synthesis of nanocrystalline LaFeO₃. *J. Mater. Chem.*, 2004, **14** (4), 764 – 69.

17. Dohnalová, Z.; Šulcová, P. & Trojan, M. Synthesis and characterization of LnFeO₃ pigments. *J. Thermal Anal. Calorim.*, 2008, **91**(2), 559-63.

18. Striker, T. & Ruud, J. A. Effect of fuel choice on the aqueous combustion synthesis of lanthanum ferrite and lanthanum manganite. *J. Amer. Ceram. Soc*., 2010, **93** (9), 2622– 2629.

19. Jain, S.R. & Adiga, K.C. A new approach to thermo chemical calculations of condensed fuel-oxidizer mixtures. *Combust. Flame*, 1981, **40**, 71-79.

20. Goldschmidt, V.M.; Barth, T.; Lunde, G. & Zachariasen, W. Geochemische. verteilungsgesetze der elemente.VII. die setze der Krystallchemie,skrifter norske videnskaps akad, Mat Naturv VolKl ,Oslo., 1926, **2** (1), 117.

21. Müller, U. Inorganic structural chemistry. 2nd ed., B.G. Teubner Stuttgart, Wiley & Sons Ltd, 1992.

22. Liu, X.C.; Hong, R. & Tian, C. Tolerance factor and the stability discussion of ABO_3 type ilmenite. J. *Mater. Sci. Mater. Electron.*, 2009, **20** (4), 323–27.

23. Qi, X.W.; Zhou, J.; Yue, Z.X.; Gui, Z.L. & Li, L.T. Auto combustion synthesis nanocrystalline *LaFeO₃. Mater. Chem. Phys.*, 2003, **78** (1), 25-29.

24. Ahmadv, H.; Salamati, H.; Kameli, P.; Poddar, A.; Acet, M. & Zakeri, K. Exchange bias in LaFeO₃ nanoparticles. *J. Phys. D. Appl. Phys.*, 2010, **43**(24), 1-5.

25. Hui, S.; Jiayue, X. & Anhua, W. Preparation and characterization of perovskite REFeO₃ nanocrystalline powders. *J. Rare Earths.*, 2010, **28**(3), 416-19.

26. Traves, D. Magnetic studies of some orthoferrites. *Phys. Rev.*, 1962, **125** (6), 1843- 53.

27. Iqbal, M.J.; Ashiq, M.N.; Gomez, P.H. & Munoz J.M. Magnetic physical and electrical properties of Zr–Ni-substituted co-precipitated strontium hexaferrite nanoparticles. *Scripta. Mater.*, 2007, **57**(12),1093–96.

28. Eivari, H.A.; Rahadr, A. & Arabi, H. Preparation of superparamgnetic iron oxide Nanoparticles and investigation their magnetic properties. *Int. J. Sci. Eng. Inves.*, 2012, **1**(3), 70-72.

29. López, M.T.L.; Durán, J.D.G.; Delgado, A.V. & Caballero, F. G. Stability and magnetic characterization of oleate covered magnetite ferrofluids in different nonpolar carriers. *J. Colloid Interface Sci.*, 2005, **291**(1), 144-151.

30. Yakushiji, K.; Mitani, S.; Takanashi, K.; Ha, J.G. & Fujimori, H. Composition dependence of particle size distribution and giant magnetoresistance in Co-Al-O granular films. *J. Magn. Magn. Mater*., 2000, **212**(1-2)75-81.

Contributors

Mr Purushottam A. Desai did his MSc in Organic Chemistry. He has been doing doctoral research under guidance of Dr (Mrs) Anjali A. Athawale. His topic of research includes synthesis and characterization of noble metal doped perovskites for catalysis applications.

Dr (Mrs) Anjali A. Athawale is an Associate Professor in the Department of Chemistry, University of Pune, India. She has been working on conducting polymers, metal nanoparticles, oxide–polymer nanocomposites and their applications as sensors as well as catalysts. She has published more than 80 research papers in international journals and has contributed a chapter in Encyclopedia of Sensors published by American Scientific Publishers.